Proceedings of the ASME 2010 3rd Joint US-European Fluids Engineering Summer Meeting and 8th International Conference on Nanochannels, Microchannels, and Minichannels
FEDSM-ICNMM2010
August 1-5, 2010, Montreal, Canada

FEDSM-ICNMM2010-31148

FLUID MECHANICS OF DEFORMABLE AORTIC PROSTHESES

Marco D. de Tullio*
DIMeG & CEMeC
Politecnico di Bari
Bari, 70125, Italy
Email: m.detullio@poliba.it

Roberto Verzicco
DIM
Universitá Tor Vergata di Roma
Roma, 00133, Italy
Email: verzicco@uniroma2.it

Luciano Afferrante
Giuseppe Pascazio
DIMeG & CEMeC
Politecnico di Bari
Bari, 70125, Italy
Email: luciano@poliba.it
Email: pascazio@poliba.it

ABSTRACT

The simultaneous replacement of a diseased aortic valve, aortic root and ascending aorta with a composite graft equipped with a prosthetic valve is a nowadays standard surgical approach in which the Valsalva sinuses of the aortic root are sacrificed and the coronary arteries are reconnected directly to the graft (Bentall procedure). In practice, two different polyethylene terephthalate (Dacron) prostheses are largely used by surgeons: a standard straight graft and a graft with a bulged portion that better reproduces the aortic root anatomy (Valsalva graft). The aim of the present investigation is to study the effect of the graft geometry, with its pseudo-sinuses, on the the flowfield, with particular attention to the coronary entry-flow, and on the stress concentration at the level of coronary-root anastomoses during the cardiac cycle. A bi-leaflet mechanical valve with curved leaflets is considered, attached to the two different prostheses. Two cylindrical channels, reproducing the very early coronary vasculature are connected to the grafts. An accurate three-dimensional numerical method, based on the immersed boundary technique, is proposed to study the flow inside deformable geometries. Direct numerical simulations of the flow inside the prostheses under physiological pulsatile inflow conditions are presented. The dynamics of the leaflets (considered rigid) is obtained by a fully-coupled fluid-structure-interaction approach, while a weak-coupled approach is employed for the deforming roots, in order to reduce the computational cost, using optimized solvers for both the fluid and structural problems. The Dacron material is modeled as orthotropic, with an inversion of the material properties in longitudinal and circumferential direction for the skirt region of the Valsalva prosthesis. Coronary perfusion is reproduced modulating in time the porosity, and thus the resistance, of the coronary channels. The results indicate that while the pseudo-sinuses do not significantly influence the coronary entry-flow, their presence allows for smaller levels of stresses at the level of coronary-root anastomoses, potentially reducing post-operative complications.

INTRODUCTION

The aortic valve is located just downstream of the heart's major pumping chamber, the left ventricle, and corresponds to the beginning of the aorta. As the heart contracts, oxygen-rich blood is forced through the open aortic valve into the aorta and it distributes nutrients to the whole body via the primary cardiovascular network. In the initial tract of the aorta, namely the aortic root, three sinuses (sinuses of Valsalva) are present, from two of whom the coronary arteries originate. These small arteries have a great clinical relevance because they are responsible for carrying oxygen-rich blood to the heart muscle itself. The Bentall procedure [1] is the standard operation for patients who have lesions of the ascending aorta associated with aortic valve disease. In fact, when a disease affects simulataneously the aortic valve, the aortic root and the ascending aorta, the risk of aortic dissection or

*Address all correspondence to this author.

rupture is greater than that associated with surgery, therefore the standard choice is to totally replace the root and ascending aorta by means of a polyethylene terephthalate (Dacron) graft carrying a prosthetic valve. In younger individuals, without contraindications to anticoagulation, mechanical valves are preferred due to their durability, thus requiring lifelong anticoagulation therapy. This routinely performed procedure provides a better annular stabilization combined with a superior support of the aortic wall. On the other hand, the root looses any extensibility because of the material with different elastic characteristics (more rigid) with respect to the native aorta. A very delicate and important step of the procedure is the re-connection of the previously separated coronary arteries to the graft, as close as possible to their natural position. This procedure may have intra-operative (bleeding) and post-operative (bleeding and late pseudo-aneurysm formation) complications due to the high torsion or tension at the level of the coronary-root anastomoses. Failure of the coronary arteries, and the consequent inability to supply adequate oxygenated blood to the heart muscle (ischaemia, myocardial infarction) is the cause of more morbidity and mortality in Western society than any other disease [2].

In the present study, two different prosthesis used in practice by surgeons are considered, equipped with a bi-leaflet mechanical valve with curved leaflets. Two cylindrical channels, reproducing the very early coronary vasculature are connected to the grafts. Coronary perfusion is reproduced modulating in time the porosity, and thus the resistance, of the coronary channels. Dacron material is modeled as orthotropic, with an inversion of the material properties in longitudinal and circumferential direction for the Valsalva prosthesis. Here we present an accurate numerical method to study the flowfield inside such deformable geometries, with the aim of studying the influence of the prosthesis type on coronary entry-flow, and to evaluate the stress concentration at the level of coronary-root anastomoses during the cardiac cycle. Pulsatile conditions involve laminar flow at the beginning, transition to turbulence at peak of flowrate and subsequent relaminarization within the same cardiac cycle. Therefore, a direct numerical simulation (DNS) technique is used, in order to correctly capture the physics of the transitional flow without introducing numerical viscosity or other artificial dissipation mechanisms. The immersed boundary (IB) technique is employed in order to easy handle complex moving and deforming geometries: The procedure is more accurate and less expensive than a standard body–fitted approach avoiding the re-meshing of the time variable computational domain with the associated interpolation step. A fully-coupled fluid-structure-interaction (FSI) approach is employed in order to correctly describe the leaflets' dynamics, while a finite-element (FE) solver for the deforming roots is coupled with the fluid solver in a segregated weak approach, in order to reduce the computational cost and to use optimized solvers for both the fluid and structural problems. Simulations of the flow inside the prostheses under physiological pulsatile inflow conditions are presented, considering several complete cardiac cycles. The results indicate that while the pseudo-sinuses do not significantly influence the coronary entry-flow, their presence allows for smaller levels of stresses at the level of coronary-root anastomoses, potentially reducing post-operative complications mainly represented by pseudoaneurysm formation at the coronary suture line.

(a) (b)

Figure 1. AORTIC DACRON PROSTHESES: (a) STRAIGHT GRAFT; (b) VALSALVA GRAFT

PROBLEM FORMULATION

Geometries

Performing the Bentall procedure, surgeons can choose two kinds of prostheses. One is the standard straight graft, a tube that has a constant orientation of the textile for the whole length, showing crimps in horizontal direction, which allow the tube to extend in the flow direction (Fig. 1a). The other is the Valsalva one, that exhibits three main portions, namely the collar, the skirt and the body. While the collar and the body have the same properties of the straight tube prosthesis, the skirt is created by taking a section of graft and sewing it to the body with crimps in vertical rather than horizontal direction. In this way, the crimp orientation of the skirt allows for larger deformation in circumferential direction, thus creating a bulged portion that better reproduces the aortic root anatomy during functioning (Fig. 1b).

Figure 2 shows the geometrical model used in the numerical simulations. The model is discretized by triangular elements, as requested by the ray–tracing technique used in the geometrical preprocessor [3]. The inflow tube and the valve housing are considered rigid, and discretized by about 2000 and 1500 elements respectively. About 100, 2200, 7300 and 5500 linear elastic shell elements, for the collar, the skirt, the body and the coronaries respectively are used in order to discretize the deformable part of the model, with six degrees of freedom for each node and thickness equal to 0.3 *mm*. The elements have both bending and membrane capabilities and support large deflection analysis. The same geometrical model is considered for both grafts, while the different behavior of the two ducts in the skirt region is taken

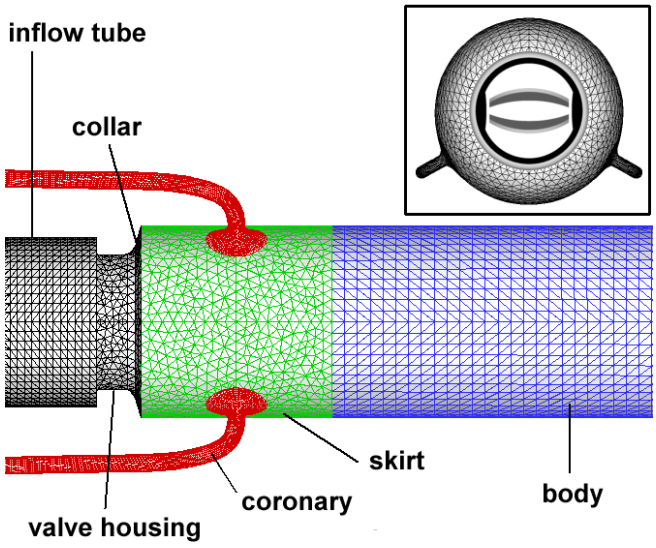

Figure 2. GEOMETRICAL MODEL AND VALVE/ROOT ARRANGEMENT

into account by a different material model. The valve considered is a bi-leaflet 25 mm Bicarbon mechanical valve by Sorin Biomedica [4]. The leaflets have a curved profile, creating three equal-resistance flow regions when open, and exhibit a rotation range equal to 60°, with a fully open position of 10° with respect to the streamwise direction. In modeling the valve, the microscopic hinge mechanism has been neglected, while a small gap of about 340 μm in the hinge region has been left in order to allow the washing flow that occurs in the real mechanism. Friction in the hinges has been neglected. About 3000 elements are used for each leaflet, considered rigid. The valve orientation with respect to the two coronaries is shown in Fig. 2. The relevant lengths of the model are reported in Fig. 3.

Materials

Dacron prosthesis have a different behavior in longitudinal and circumferential direction, therefore are characterized by orthotropic material properties in the present work. As shown in [5], the stress-strain relation for the woven Dacron graft can be correctly modeled with a linear model both in longitudinal and circumferential directions. Considering z axis in the flow direction, nine elastic constants (Young's moduli E_x, E_y, E_z, Poisson's ratios ν_{yz}, ν_{zx}, ν_{xy}, and shear moduli G_{yz}, G_{zx}, G_{xy}) need to be defined and for the compliance matrix to be positive definite the following condition must be satisfied:

$$1-\nu_{xy}^2\frac{E_y}{E_x}-\nu_{yz}^2\frac{E_z}{E_y}-\nu_{xz}^2\frac{E_z}{E_x}-2\nu_{xy}\nu_{yz}\nu_{xz}\frac{E_z}{E_x}>0 \qquad (1)$$

Table 1. NUMERICAL VALUES OF THE MATERIAL CONSTANTS FOR THE DEFORMABLE GRAFT.

$E_x=E_y$	E_z	$\nu_{xz}=\nu_{yz}$	ν_{xy}	$G_{xz}=G_{yz}$	G_{xy}
12 *MPa*	1.2 *MPa*	0.15	0.1	5.2 *MPa*	0.55 *MPa*

Since the Dacron graft can be considered as transversely isotropic ($E_x=E_y$, $\nu_{xz}=\nu_{yz}$, $G_{xz}=G_{yz}$), the elastic constants are actually six. Under this assumption we compute $G_{xz}=E_x/2(1+\nu_{xz})$. Concerning G_{xy}, results showed that stresses and strains are negligibly affected by its value, so the value $E_x/2(1+\nu_{xy})$ is considered. Numerical values of the material constants, deduced by the experimental stress-strain curves reported in [5] are shown in Tab. 1. It is worth noting that for the Valsalva graft, the orthotropic directions of the material are inverted at the skirt region, in order to take into account the different behavior of the prosthesis.

A linear elastic material with Young's modulus equal to 2 *MPa* was used for the two coronaries. This value gives a good match, in terms of displacement and strain results, with respect to more sophisticated models, adopted in literature to model the natural aortic root, that use non–linear material properties [6]. The inflow tract, including the valve housing ($\partial\Gamma_1$ in Fig. 3), is considered rigid and fixed in space. The leaflets are considered rigid and made by pyrolytic carbon, with density of $\rho_l=2000\ kg/m^3$. Eeach leaflet has a moment of inertia with respect to the pivot axis of $7.947\times10^{-9}\ kg\cdot m^2$.

Flow and structural solvers

In every point of the time–dependent fluid domain Γ (see Fig. 3), the Navier–Stokes equation for an incompressible viscous Newtonian fluid are solved:

$$\nabla\cdot\mathbf{u}=0, \qquad (2)$$

$$\frac{\partial\mathbf{u}}{\partial t}+\nabla\cdot(\mathbf{uu})=-\nabla p+\frac{1}{Re}\nabla^2\mathbf{u}+\mathbf{f}+\mathbf{f}', \qquad (3)$$

where $\mathbf{u}$ is the velocity vector, p is the pressure, $\mathbf{f}$ is the direct forcing term of the immersed boundary method [7], $\mathbf{f}'$ is the forcing term for the coronary arteries, and *Re* is the Reynolds number. Both $\mathbf{f}'$ and *Re* are later specified. The two leaflets, L_i can rotate about their own pivots and their angular displacements θ_i are governed by the following equations:

$$I_i\frac{d^2\theta_i}{dt^2}=T_i, \qquad \text{for } L_i \quad \text{with} \quad i=1,2, \qquad (4)$$

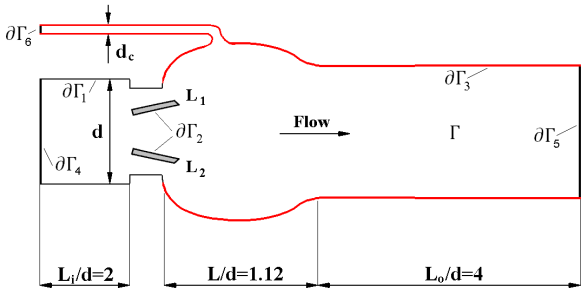

Figure 3. SKETCH OF COMPUTATIONAL DOMAIN ($d = 25\,mm$, $d_c = 3\,mm$). THE RED LINES INDICATE THE DEFORMABLE REGION.

where I_i are the moment of inertia about the pivots and T_i are the tilting moments about the pivots resulting from the viscous stress tensor τ and the pressure integrated over the leaflets surfaces S_i. The incompressible Navier-Stokes equations are discretized in space using second-order-accurate central differences in conservative form and in cylindrical coordinates [8]. The resulting system is solved using a fractional–step method, where the viscous terms are computed implicitly and the convective terms explicitly. The large–banded matrix associated with the elliptic equation is reduced to a penta–diagonal matrix using trigonometric expansions (FFT's) in the azimuthal direction and the resulting Helmholtz equations are then inverted using the FISHPACK package [9]. A third-order Runge–Kutta scheme is used to advance the equations in time. All the results have been obtained with a fixed Courant number equal to 0.25 thus having a variable time step Δt that is adjusted accordingly. Small time steps occur during opening and closing of the leaflets, thus allowing an accurate simulation of these phases, while larger time steps typically occur after valve closure, when the mean flow is essentially zero and the leaflets still. More details on the Navier–Stokes solver and the IB technique are given in [7, 8, 10].

The Navier equation governs the dynamics of the solid region ($\partial\Gamma_3$ in Fig. 3):

$$\nabla \cdot \sigma_s = \rho_s \frac{\partial^2 \mathbf{u}_s}{\partial t^2} \tag{5}$$

where σ_s is the stress tensor, ρ_s and $\mathbf{u}_s$ are the density and velocity of the solid respectively. The constitutive relation between the stress and strain is given by:

$$\sigma_s = \mathbf{C}\mathbf{E}_s \tag{6}$$

where $\mathbf{C}$ is the elasticity tensor and

$$\mathbf{E}_s = \frac{1}{2}\left[\nabla \mathbf{u}_s + (\nabla \mathbf{u}_s)^T + (\nabla \mathbf{u}_s)^T \nabla \mathbf{u}_s\right] \tag{7}$$

is the strain tensor. The finite-element commercial software ANSYS® Multiphysics™ [11] is used to solve the above equations. It is worth noting that, in the present work the unsteady terms of equation (5) are not considered, thus neglecting inertial effects of the deforming structure. In particular, since the blood is assumed incompressible, the wave propagation phenomena of the system are not captured. It turns out that this is a quasi-static approximation: the time evolution of the prosthesis is described by a sequence of static configurations. For our purpose, that is the evaluation of stress time-history of the prosthesis, we expect that this assumption does not significantly affect the results.

Fluid–structure interaction

Two different fluid–structure interaction approaches are considered for the rigid leaflets and for the deformable aortic prosthesis structure.

A strong coupling scheme is employed for the solution of the system (2)–(4) where the fluid and the structure are treated as elements of a single dynamical system, all governing equations being integrated simultaneously in the time–domain. A Hamming's 4^{th}–order predictor–corrector method as described in [12] is used to integrate equations (2)–(4) through an iterative scheme until convergence is achieved. The number of iterations required for convergence at each time step varied from 1 to 4, depending on the phase of the dynamics; convergence is typically more difficult during the opening and closing phases when the leaflets rotate very rapidly while the criterion is satisfied already at the first iteration when the leaflets remain still or move slowly. Further details on the method and several checks of the numerics can be found in [10].

Considering the deforming structure, the wall deformation and the flow problems are solved in a successive manner with a partitioned (segregated) approach. A weak-coupling is employed in order to reduce the computational cost of the procedure and to use optimized solvers for both the fluid and the structural problem. For each time step, the following procedure is employed, where n and $n+1$ indicate the time levels and subscripts f and s indicate fluid and structure's quantities:

1. the flow solver is advanced in time to obtain the new velocity and pressure fields $\mathbf{u}_f^{n+1}$ and p_f^{n+1}, imposing the position and velocity of the structure nodes $\mathbf{x}_s^n$ and $\mathbf{u}_s^n$ as boundary conditions for the fluid domain;
2. the loads exerted on the structure by the fluid $\Phi_f^{n+1} = \Phi_f^{n+1}(\mathbf{x}_s^n, \mathbf{u}_f^{n+1}, p_f^{n+1})$ are computed;
3. the structural solver is run with the computed loads, $\Phi_s^{n+1} = \Phi_f^{n+1}$ to obtain the new position and velocity of the structural nodes, $\mathbf{x}_s^{n+1}$ and $\mathbf{u}_s^{n+1}$.

In this way, the approach requires the solution of the fluid and structural problem only once per time step. Stability is en-

sured by the very small time steps required by the flow solver to capture the time-history of the smallest turbulent scales.

Modeling coronary-entry flow

The ultimate function of the coronary system is to deliver blood to the cardiac tissue, that is alternately contracting and relaxing. During systole, the contraction of the myocardium compresses the intra-myocardial capillaries, resulting in a *throttling* of these vessels. This effect ceases during diastole when the myocardium relaxes, and, although it is stretched by ventricular dilatation, the blood can better flow through the coronaries under the driving pressure gradient. This leads to a pulsatile flow in which the resistance can not be simply related to the vessel radius. Even the geometrical formulation of the problem is very difficult due to the complex architecture of the coronary network: the precise branching structure of the system, one of the most compact and complex within the human body, could be mapped for each individual up to a limited level of details, most of the coronary small vasculature being deeply embedded within the cardiac muscular tissue [2, 13]. Direct measurements of flow at the capillary output of the system are not possible, the precise number of capillaries (of the order of millions) being undeterminable as well as their flow velocity. On the other hand, some measurements are possible at the entry-level of the system, namely the left or right main coronary arteries departing from the aortic sinuses. In the absence of adequate access to the system for direct measurements of pressure and flow, simplifications are necessary in order to study this complicate system, or at least a part of it.

In this work we concentrate only on the very early vasculature of the coronary system, namely the two vessels connected to the Valsalva sinuses, assuming that everything downstream, once correctly modeled, maintains the same behavior for different aortic geometries. Therefore, by *coronary blood flow* we indicate the flow through such main vessels, entering the coronary system, that is the only flow reasonably accessible for measurements. At this level, the correctness of our model can be guided by a comparison of the results of the model in terms of flow rate with direct measurements available. We have replaced the complex branching structure of the vascular system by two identical tubes connected to the coronary ostia of the aorta in the two sinuses of Valsalva (see Fig. 2). The pressure gradient between the entrance region and the outflow of the tubes provides the driving force for the coronary flow. In order to mimic the *tissue pressure effect* [14], that is the rhythmic contractions of the myocardium within each pumping cycle, the computational region inside the coronary tubes is treated as a porous medium by adding an extra forcing term in the Navier–Stokes equation that modulates in time the porosity of the material:

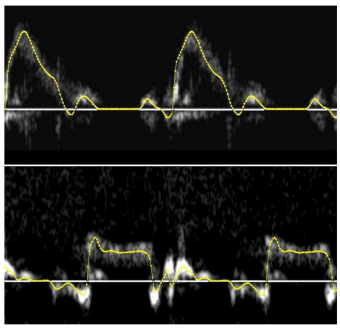

Figure 4. AORTIC (TOP) AND CORONARIC (BOTTOM) VELOCITY PROFILES BY MEANS OF PULSE WAVE DOPPLER ECHOCARDIOGRAPHY RECORDED IN VIVO IN A YOUNG HEALTHY MAN

$$\mathbf{f}' = \frac{\nu(\mathbf{u}-\mathbf{V})}{\rho\, Da\, K(t)}. \tag{8}$$

Here $Da = K_0/L^2$ is the Darcy number, with K_0 and L a reference permeability and reference length, respectively, and $K(t)$ is a time–dependent function that modulates the porosity. If $K(t) \to \infty$ the forcing vanishes and the standard Navier–Stokes equations are recovered (the fluid is allowed to flow through coronaries). If $K(t) \to 0$ the forcing becomes dominant in the equation yielding $\mathbf{u} = \mathbf{V}$: by imposing $\mathbf{V} = 0$ the no–flux condition inside the coronaries is obtained. Unfortunately, the effect of the forcing (8) on the system (3) is exactly known only for the extreme values of K that can not be used in practice. For the present computations, therefore, a *tuning* was necessary in order to modulate the resistance of the channels so as to obtain a realistic coronary flow rate. More in detail, the forcing (8) was tuned so to reproduce a physiological flow similar to that observed by Pulsed Wave Doppler echo-cardiographic recording in a human being (Fig. 4). The flow profile in this individual, a young man, has been chosen as it corresponds, by an expert cardiology judgment, to the most typically observed flow profile found in normal healthy conditions. Once $\mathbf{f}'$ has been identified as in Fig. 5 it has been maintained identical in all simulations in which the aortic root geometry or other flow details have been modified. Maintaining the same forcing through all the simulations is physically equivalent to have always the same drag of the complex vascular network downstream of the coronaries, and this is a natural assumption since the coronary network is not modified by the surgery of the aortic root. Within our hypothesis, we consider the total coronary flow behaving near the optimum conditions,

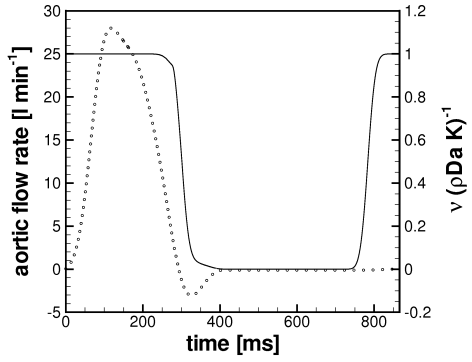

Figure 5. FORCING TERM (CONTINUOUS LINE) INSIDE CORONARIES IN FUNCTION OF TIME. AORTIC FLOW (DOTS) IS PLOTTED FOR REFERENCE

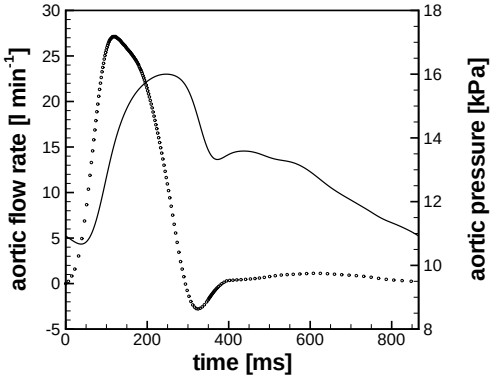

Figure 6. INFLOW AORTIC FLOWRATE (DOTS) AND PRESSURE (LINE)

dominated by resistive flow and only slightly affected by inertial and capacitive effects (see [15] for details).

Flow parameters and simulation details

Typical physiological conditions for an adult human being are considered: The cycle duration is set at 866 ms, corresponding to about 70 beats/min (natural heart rate at rest). The mean flow rate was adjusted to about 5 l/min with a peak flow rate of about 28 l/min. The blood kinematic viscosity and density are set to $\nu = 3.04 \times 10^{-6}\ m^2/s$ and $\rho_b = 1060\ kg/m^3$ respectively. The peak Reynolds number, considering the bulk velocity at the peak inflow $U = 0.95$ m/s and the inflow tube diameter $d = 25$ mm is about $Re = Ud/\nu = 7800$. The geometries describing the prosthesis, the valve and the leaflets are embedded into the background cylindrical structured grid. After a grid convergence study, it was found that the results (in terms of leaflet dynamics and velocity profiles downstream of the valve) were grid converged on the grid with $217 \times 165 \times 250$ nodes (about 9 millions points) in the azimuthal, radial and axial directions respectively. The grid is uniform in the azimuthal and radial direction, while it is non–uniform in the axial direction and clustered near the valve. Five cardiac cycles are computed for the two cases (straight tube and Valsalva). Each cycle is discretized by a variable time step ranging from $\Delta t_{min} = 3\ \mu s$ occurring at the flow rate peak, to a maximum value of $\Delta t_{max} = 250\ \mu s$ during the diastole. The CPU time for the computation of each complete cycle was equal to about 75 hours on a single P-IV processor at 2.4 *GHz*, equipped with 2 Gb of RAM for the fluid solver, while about 100 hours per cycle are needed by the structural solver.

Boundary conditions

For the fluid domain inflow section ($\partial\Gamma_4$ in Fig. 3), pressure and velocity profiles are imposed in order to mimic the physiological flow rate and pressure produced by the heart in the left ventricle, as shown in Fig. 6. The velocity profile at the nodes of the inflow section follows an hyperbolic tangent function, with stretching parameter $\gamma = 60$, which yields a flat velocity distribution in the bulk and accommodates the no–slip boundary condition at the aortic wall within a layer of thickness $\lambda/d = 1/\sqrt{Re} \simeq 1.2 \times 10^{-2}$. The regions $\partial\Gamma_5$ and $\partial\Gamma_6$ in Fig. 3 are treated as outflow sections. Concerning the deformable structure, it is fully constrained at the lowest nodes (where the mechanical valve is fixed to the prosthesis), while a longitudinal displacement is applied to the highest nodes ($\partial\Gamma_5$ in Fig. 3) to simulate the longitudinal stresses reported in natural aorta. Referring to the work of [16], where experimental investigations on canine and porcine aortas were performed, we consider a longitudinal displacement at the position of the aortic arch (corresponding in our model at the position of the highest nodes) of about 5 *mm*. This maximum displacement is modulated in time by the pressure curve depicted in Fig. 6.

At the interface between the fluid and the solid domain ($\partial\Gamma_1$, $\partial\Gamma_2$ and $\partial\Gamma_3$ in Fig. 3), the continuity of displacements, velocity (no–slip condition) and loads is imposed:

$$\mathbf{x}_f = \mathbf{x}_s; \quad \mathbf{u}_f = \mathbf{u}_s; \quad \Phi_f = \Phi_s \tag{9}$$

Validation of the fluid-structure interaction model

The validation of the fully-coupled approach of the flow solver with the equations governing the dynamics of the leaflets, considering an indeformable geometry, is presented in [10]. The comparison between leaflets' angular displacement in time with

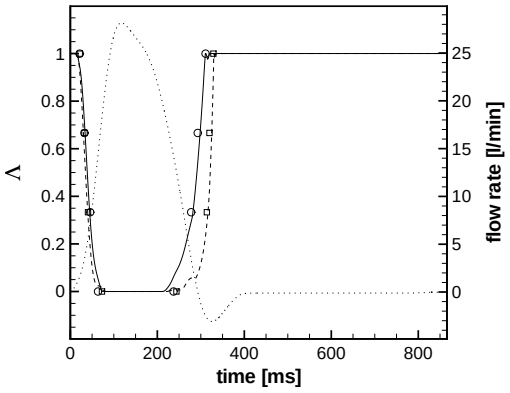

Figure 7. TIME VARIATION OF THE PHASE–AVERAGED LEAFLETS' ANGULAR POSITION $\Lambda = \frac{(\alpha_{open}-\alpha)}{(\alpha_{open}-\alpha_{closed})}$ (LINES). SYMBOLS ARE EXPERIMENTAL RESULTS OF [17]. AORTIC FLOW (DOTS) IS REPORTED FOR REFERENCE

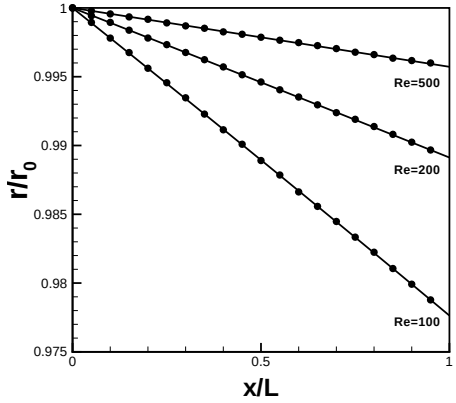

Figure 8. LAMINAR FLOW INSIDE A DEFORMABLE PIPE: PIPE RADIUS VERSUS PIPE LENGTH AT DIFFERENT REYNOLDS NUMBERS LINES ARE ANALYTICAL RESULTS, WHILE DOTS ARE NUMERICAL SIMULATION RESULTS

respect to experimental results is shown in Fig. 7. Here, the coupling of the flow solver with the deformable structure has been validated considering a non-constrained pipe conveying a fully-developed stationary flow, and comparing the results with the analytical ones reported in [18]. In order to consider a fully developed flow, and to avoid side-effects, the total pipe length considered was set to $L_{tot} = 30 \cdot d_0$, where d_0 is the diameter of the unloaded pipe, while only the central part of the tube, with length of $L = 10 \cdot d_0$, is considered for the comparison of the results. A comparison between numerical and analytical results in terms of dimensionless pipe radius r/r_0 variation with dimensionless streamwise position x/L for different Reynolds numbers is shown in Fig. 8. The agreement between numerical and analytical predictions is satisfactory.

RESULTS

The phase-averaged angular displacement of the two leaflets, for both prostheses during the cardiac cycle is shown in Fig. 9: Very little sensitivity to the aortic root geometry is observed. The leaflet dynamics is greatly influenced by the pressure gradient through the valve, and this is evident during the opening phase, where the flow is accelerated. Small differences are noticeable during the closing phase, where the deceleration of the flow promotes high turbulence, and therefore the integration of the pressure and viscous stresses over the leaflets is influenced by the fluctuations in time of the pressure and velocity fields. The leaflets closure is mainly synchronous, and it is worth noting that the asynchronous closure observed in [10] (see Fig. 7 for a three sinuses configuration) here is absent, due to the axysimmetry of the geometries.

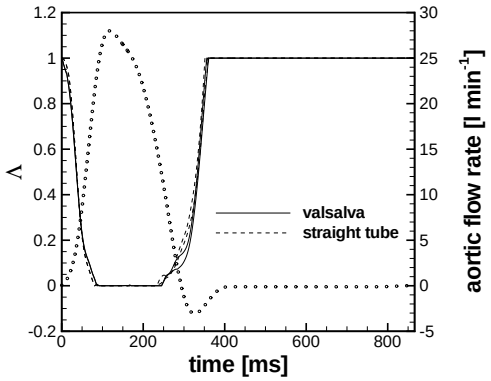

Figure 9. TIME VARIATION OF THE PHASE–AVERAGED LEAFLETS' ANGULAR POSITION $\Lambda = \frac{(\alpha_{open}-\alpha)}{(\alpha_{open}-\alpha_{closed})}$

Out-of-plane vorticity contours in the symmetry plane are shown in Fig. 10, at three significant instant: i)) start opening of the leaflets; ii) flow rate peak; iii) start closure of the leaflets. The typical configuration of the bi-leaflet valves, forming three jets, with strong shear layers shed from the valve housing and the tips of the leaflets is noticeable. At the peak of flow rate, the shear layers become unstable and a strong small-scale turbulence production is observed in the wake and in the sinuses region. Both straight and Valsalva prosthesis exhibits an axysimmetric recirculation region due to the sudden expansion that the flow encounters crossing the valve, whereas this region is less pronounced in the straight tube case. During the decelerating

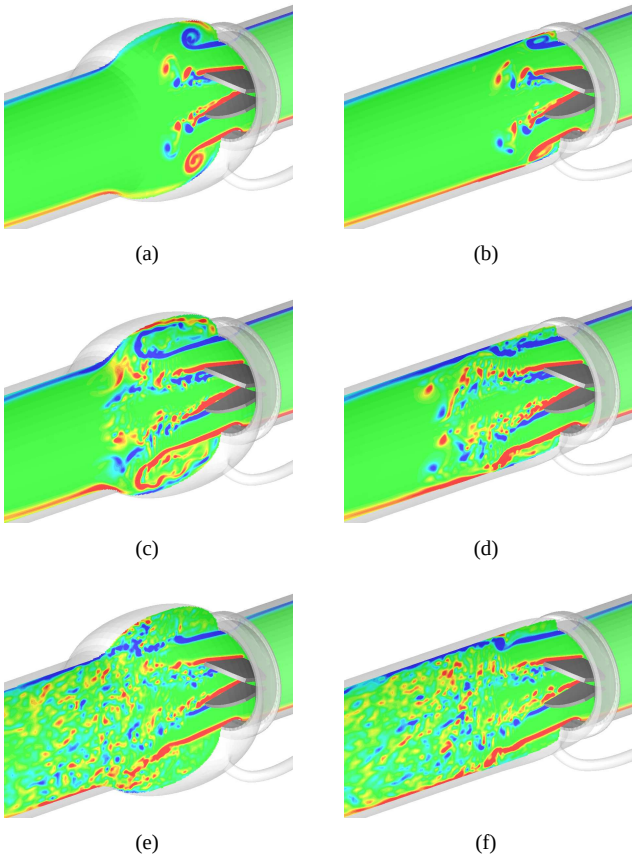

Figure 10. OUT OF PLANE VORTICITY IN THE SYMMETRY PLANE FOR THE VALSALVA (LEFT) AND STRAIGHT (RIGHT) GRAFTS: (a)-(b) START OPENING OF THE LEAFLETS; (c)-(d) FLOW RATE PEAK; (e)-(f) START CLOSURE OF THE LEAFLETS

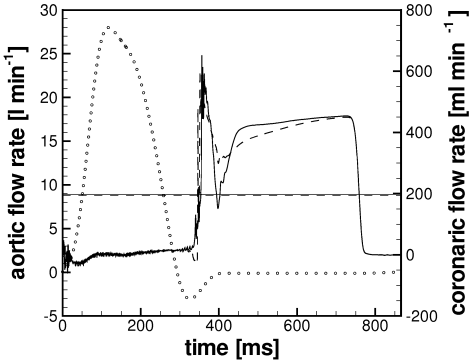

Figure 11. PHASE-AVERAGED AND MEAN CORONARY FLOW RATE. CONTINUOUS LINES INDICATE THE VALSALVA CASE; WHILE DOTTED LINES INDICATE THE STRAIGHT TUBE. AORTIC FLOW (DOTS) IS REPORTED FOR REFERENCE

Table 2. RELATIVE DEFORMATION OF THE PROSTHESES DIAMETER AT THE MIDDLE SECTION OF SINUS REGION, WITH RESPECT TO THE UNLOADED CASE.

	straight tube	Valsalva tube
systolic	7.67 %	49.6 %
diastolic	5.56 %	34.0 %

phase the flow become turbulent with high production of small scale structures downstream the valve. The leaflet start closing under the adverse pressure gradient until complete closure. After valve closure the main flow is essentially zero, therefore viscosity dissipates the small scale structures until the beginning of the new cycle.

Figure 11 shows the computed total coronary blood flow. In this configuration, the computed mean coronary flow (little below 200ml/s) is close to the upper level of the physiological flow range, that can be up to about 5% of the aortic flow [19], that for our setup is about 250 ml/min. The two configurations provide essentially the same mean flow rate: 193.8 ml/min and 187.21 ml/min for the Valsalva and straight graft respectively, showing that the presence of pseudo-sinuses does not influence the coronary flow. These results are in agreement with the *in vivo* observations of [20].

Table 2 reports the relative deformation of the prostheses diameter with respect to the unloaded case, in a section corresponding to the middle of the sinus region. The diameter variation is very small in the region where the crimps are horizontal, namely for the straight tube and for the body of the Valsalva prosthesis, whereas it is larger in the skirt region, where the crimps are longitudinal, the tube taking the shape of a quasi-axisymmetric bulb. In Fig. 12 the Von Mises stress near the coronary root anastomoses is reported, plotted versus time for a cardiac cycle and for both the prostheses. The straight tube graft experiences the largest stresses, with a value of the maximum stress that is 2 time higher than the Valsalva prosthesis. It is worth noting that the stress peak at coronary–root anastomoses after valve closure is greatly reduced in the straight tube because of its more rigid structure. Finally contour maps of the Von Mises stress distribution for both prostheses are plot in Fig. 13, at the minimum and maximum pressures registered during cardiac cycle. The maps clearly show how the stress values, in the region corresponding to the sinuses, are smaller for the Valsalva prosthesis than the straight one. It is worth noting that higher values of the stresses are found near the sinotubular junctions, but this raises no concern because this zone is not prone to rupture

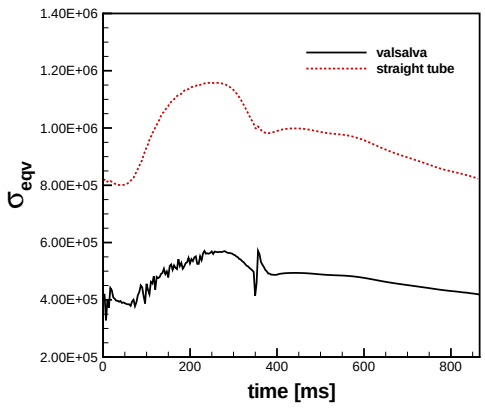

Figure 12. VON MISES STRESS VERSUS TIME IN A REGION NEAR THE CORONARY ROOT ANASTOMOSIS

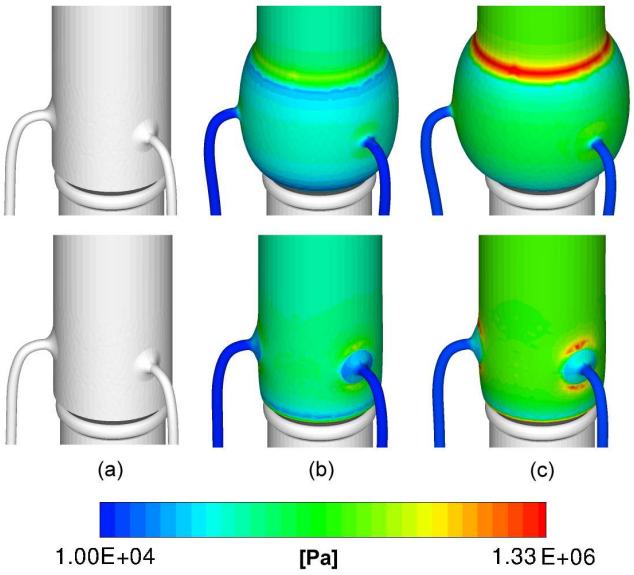

Figure 13. (a) UNLOADED CONFIGURATION AND VON MISES STRESS CONTOURS AT MINIMUM (B) AND MAXIMUM (C) LEVELS OF PRESSURE DURING A CARDIAC CYCLE FOR THE VALSALVA (TOP) AND STRAIGHT (BOTTOM) GRAFTS.

(being an all-Dacron component reinforced by machine suturing during the manufacturing), differently from the hand-sewn coronary root anastomoses. The lower stresses found for the Valsalva prosthesis is a suitable result that could reduce complications like the bleeding and the pseudoaneurysm formation in the region of coronary-root anastomoses.

CONCLUSIONS

In this paper an accurate numerical method to study the flowfield inside deformable geometries is presented. The use of the immersed boundary technique allows one to handle complex moving and deforming geometry in an efficient way, maintaining the computational grid fixed in space, with no need for regenerating it at each time step. A direct numerical simulation method is chosen for describing the flow behavior. Two fluid-structure-interaction approaches are employed in order to study the solids' dynamics: a fully-coupled approach for rigid bodies moving inside the computational domain, and a weak-coupling approach for deforming structures. The approach presented is used to study the flowfield inside two type of aortic prostheses used in practice by surgeons, when a disease affects simultaneously the aortic valve, aortic root and ascending aorta: a straight tube, and a Valsalva tube with a bulged portion in the region where the natural sinuses are present. Both the prostheses considered are equipped with a bileaflet mechanical heart valve. Also the stress concentration near the junction of the coronary arteries to the prostheses, that is prone to rupture in the real case, is evaluated. The prostheses' material considered is Dacron, modeled as orthotropic, with an inversion of the orthotropic directions in the sinus region for the Valsalva prosthesis. Several complete cardiac cycles are studied, under pulsatile physiological conditions. Leaflets' motion and coronary entry flow are only slightly affected by the prosthesis type, while stress concentration found near the coronary root anastomoses is higher, by a factor of two, for the straight tube prosthesis, this indicating that the Valsalva one should be preferable in practice, reducing the risk of complications like pseudo-aneurysm formation at the coronary suture lines.

ACKNOWLEDGMENT

This research was funded by by MIUR and Politecnico di Bari under contract CofinLab 2001.

REFERENCES

[1] Bentall, H., and De Bono, A., 1968. "A technique for complete replacement of the ascending aorta". *Thorax,* ***23***, pp. 338–339.

[2] Nichols, W. W., and O'Rourke, M. F., 1990. *McDonald's blood flow in arteries.* Lea & Febiger, Philadelphia, PA.

[3] Iaccarino, G., and Verzicco, R., 2003. "Immersed boundary technique for turbulent flow simulations". *Appl. Mech. Rev.,* ***56***, p. 331.

[4] Sorin-Group, 2006. Sorin Biomedica. http://www.sorinbiomedica.com.

[5] Lee, J., and Wilson, G., 1986. "Anisotropic tensile viscoelastic properties of vascular graft materials tested at low strain rates". *Biomaterials,* ***7***, pp. 423–431.

[6] Ranga, A., Mongrain, R., Mendes Galaz, R., Biadillah, Y., and Cartier, R., 2004. "Large–displacement 3d structural analysis of an aortic valve model with nonlinear material properties". *Journal of Medical Engineering & Technology,* ***28***, pp. 95–103.

[7] Fadlun, E. A., Verzicco, R., Orlandi, P., and Mohd-Yosuf, J., 2000. "Combined immersed-boundary finite-difference methods for three-dimensional complex flow simulations". *J. Comput. Phys.,* ***161***, p. 35.

[8] Verzicco, R., and Orlandi, P., 1996. "A finite difference scheme for threedimensional incompressible flows in cylindrical coordinates". *Journal of Computational Physics,* ***123***, pp. 402–413.

[9] Swartzrauber, P., N., 1974. "A direct method for the discrete solution of separable elliptic equations". *SIAM J. Numer. Anal.,* ***11***, p. 11361150.

[10] de Tullio, M., Cristallo, A., Balaras, E., and Verzicco, R., 2009. "Direct numerical simulation of the pulsatile flow through an aortic bileaflet mechanical heart valve". *Journal of Fluid Mechanics,* ***622***, pp. 259–290.

[11] ANSYS®, 2009. ANSYS, Inc. http://www.ansys.com.

[12] Yang, J., Preidikman, S., and Balaras, E., 2008. "A strongly–coupled embedded boundary method for fluid–structure interaction of elastically mounted rigid bodies". *J. Fluids and Structures,* ***182***, pp. 167–182.

[13] Attinger, E., 1963. *Pulsatile flow*. McGraw-Hill, New York.

[14] Kajiya, F., Matsuoka, S., Ogasawara, Y., Hiramatsu, O., Kanazawa, S., Wada, Y., Tadaoka, S., Tsujioka, K., Fujiwara, T., and Zamir, M., 1993. "Velocity profiles and phasic flow patterns in the non-stenotic human left anterior descending coronary artery during cardiac surgery". *Cardiovascular Research,* ***27***, pp. 845–850.

[15] Zamir, M., 2005. *The Physics of Coronary Blood Flow*. Springer.

[16] Han, H., and Fung, Y., 1995. "Longitudinal strain of canine and porcine aortas". *J. of Biomechanics,* ***28***, pp. 637–641.

[17] Cerroni, G., 2006. "Studio sperimentale del campo fluidodinamico a valle di una valvola cardiaca artificiale e in un dispositivo di circolazione assistita mediante tecnica PIV". Master's thesis, Universita' degli studi di Roma, La Sapienza, Facolta' di Ingegneria.

[18] Fung, Y., 1984. *Biodynamics. Circulation*. Springer-Verlag, New York Berlin Heidelberg Tokyo.

[19] Folkow, B., and Neil, E., 1971. *Circulation*. Oxford University Press, New York.

[20] De Paulis, R., Tomai, F., Bertoldo, F., Ghini, A., Scaffa, R., Nardi, P., and Chiarello, L., 2004. "Coronary flow characteristics after a Bentall procedure with or without sinuses of Valsalva". *European journal of cardio-thoracic surgery,* ***26***, pp. 66–72.